

# Optical study of $\text{La}_3\text{Ga}_{5.5}\text{Ta}_{0.5}\text{O}_{14}$ single crystal co-doped with $\text{Ho}^{3+}$ and $\text{Yb}^{3+}$

Radosław Lisiecki · Witold Ryba-Romanowski ·  
Lucyna Macalik · Jarosław Komar ·  
Marek Berkowski

Received: 4 June 2013 / Accepted: 26 September 2013 / Published online: 22 October 2013  
© Springer-Verlag Berlin Heidelberg 2013

**Abstract** Single crystal of  $\text{La}_3\text{Ga}_{5.5}\text{Ta}_{0.5}\text{O}_{14}$  (LGT) containing intentionally 0.5 % of  $\text{Ho}^{3+}$  and 1 % of  $\text{Yb}^{3+}$  was grown by the Czochralski method. Examination of chemical composition of the grown crystal revealed that luminescent holmium and ytterbium ions are preferably retained in the melt and their actual concentrations are 0.12 and 0.24 %, respectively. Spectroscopic investigation performed encompassed IR host absorption spectra and Raman spectra at room temperature, optical absorption and luminescence spectra of  $\text{Ho}^{3+}$  and  $\text{Yb}^{3+}$  at room temperature and at 5 K, and luminescence decay curves at room temperature. It was found that all spectral bands recorded show important inhomogeneous line broadening. This feature was attributed to structural disorder inherent to the crystal lattice in which pentavalent  $\text{Ta}^{5+}$  ions occupy octahedral Ga(1) sites together with trivalent  $\text{Ga}^{3+}$  ions. Despite small concentrations of luminescent ions, the occurrence of nonradiative interaction that feeds the  $^5\text{I}_6$  and  $^5\text{I}_7$  levels of  $\text{Ho}^{3+}$  ions by transfer of an excitation from the  $^2\text{F}_{5/2}$  level of  $\text{Yb}^{3+}$  ions was evidenced. Based on examination of spectroscopic parameters evaluated, it was concluded that LGT:Ho, Yb may be considered as a potential intermediate-gain laser active material able to emit infrared radiation from the  $^5\text{I}_7 \rightarrow ^5\text{I}_8$  transition of  $\text{Ho}^{3+}$  around 2 micrometres upon laser-diode pumping into  $\text{Yb}^{3+}$  absorption band.

## 1 Introduction

Interest in holmium-doped crystals and glasses is stimulated by their potential for a laser operation in near infrared region. Infrared transitions originating in metastable levels  $^5\text{I}_7$  and  $^5\text{I}_6$  of  $\text{Ho}^{3+}$  ions are favourable for this purpose. Main attention in published works has been devoted to the  $^5\text{I}_7 \rightarrow ^5\text{I}_8$  transition around 2  $\mu\text{m}$ . Nevertheless, the ability of  $\text{Ho}^{3+}$  ions to show laser operation associated with the  $^5\text{I}_6 \rightarrow ^5\text{I}_7$  transition around 2.9  $\mu\text{m}$ , and the  $^5\text{I}_6 \rightarrow ^5\text{I}_8$  transition around 1.2  $\mu\text{m}$  has been demonstrated [1]. The fundamental obstacle in the development of infrared holmium lasers stems from the lack of absorption bands with appreciable intensity that can serve as pump bands. Therefore, holmium-doped materials have to be co-doped by sensitizer ions able to absorb incident pump radiation and transfer acquired excitation energy to holmium ions. Besides trivalent thulium ions, the most frequently ytterbium ions are considered for this purpose since the  $^2\text{F}_{7/2} \rightarrow ^2\text{F}_{5/2}$  absorption band of  $\text{Yb}^{3+}$  matches perfectly emission spectra of commercial high-power laser diodes. Indeed, numerous published works have dealt with the  $\text{Ho}^{3+} + \text{Yb}^{3+}$  system in various hosts, among others in  $\text{Y}_3\text{Sc}_2\text{Ga}_3\text{O}_{12}$  [1],  $\text{YAl}_3(\text{BO}_3)_4$  [2],  $\text{KLu}(\text{WO}_4)_2$  [3],  $\text{YVO}_4$  [4] crystals, tellurite glass [5], germanate glass [6] or  $(\text{YLa})_2\text{O}_3$  transparent ceramics [7]. In this work, spectral characteristics and dynamics of excited states relevant to a potential infrared laser operation in  $\text{La}_3\text{Ga}_{5.5}\text{Ta}_{0.5}\text{O}_{14}$  (LGT) single crystal co-doped with  $\text{Ho}^{3+}$  and  $\text{Yb}^{3+}$  are reported. Crystal structure and fundamental physicochemical properties of LGT host crystal are known for a long time. It has been ascertained that LGT forms optically uniaxial crystals belonging to the P321 space group [8]. In this structure, the La, Ga and Ta cations are surrounded by oxygen ions and reside in different structural units [9–11].

R. Lisiecki (✉) · W. Ryba-Romanowski · L. Macalik ·  
J. Komar  
Institute of Low Temperature and Structure Research, Polish  
Academy of Sciences, Okolna 2, 50-422 Wrocław, Poland  
e-mail: R.Lisiecki@int.pan.wroc.pl

M. Berkowski  
Institute of Physics, Polish Academy of Sciences,  
Al. Lotnikow 32/46, 02-668 Warsaw, Poland

$\text{La}^{3+}$  ions are located in Thomson cubes and occupy sites with  $C_2$  symmetry. There are three different positions of  $\text{Ga}^{3+}$  ions: trigonal–pyramidal Ga(3), tetrahedral Ga(2) and octahedral Ga(1). The latter position is occupied in part by  $\text{Ta}^{5+}$  ions, thereby giving rise to a certain structural disorder.

Much attention has been directed to master the LGT crystal growth by the Czochralski technique [10, 12, 13]. In particular, dependence of the chemical composition and oxygen deficiency in fabricated crystals on growing atmosphere, type of crucible and direction of growth has been determined [10, 13]. Investigation of physicochemical features of LGT crystals has revealed that they show piezoelectric and electro-optic properties significantly much better than those of  $\alpha$ -quartz and have a significant optical activity [12, 14]. It has been pointed out also that LGT crystals have a potential for application in acousto-electronic devices [12, 14].

Literature concerning optical properties of rare earth-doped LGT crystals is not abundant. Some spectroscopic features and laser performance of a laser-diode-pumped LGT: $\text{Nd}^{3+}$  system have been reported in the past [15]. Later on, transition intensities and excited state relaxation dynamics of erbium-doped LGT single crystals have been studied [16]. In recent papers, luminescence characteristics of polycrystalline europium-doped LGT phosphors [17] and phenomena of up-conversion of infrared radiation into visible luminescence in LGT powders co-doped with erbium and ytterbium [18] have been considered.

Intention of the present study is to gain an insight into spectroscopic features of the system under study relevant to its potential for the design of a laser-diode-pumped infrared lasers operating near 2 micrometres.

## 2 Experimental

Single crystal of LGT with intentional concentrations  $C_{\text{Ho}} = 0.5$  at.% and  $C_{\text{Yb}} = 1$  at.% was grown by the Czochralski method from iridium crucibles. The crystal was pulled along  $c$  crystallographic axis. This growing direction was chosen since previous experimental approaches made it possible to ascertain that although boules grown contain an inevitable central core, the remaining volume of the crystal has excellent optical quality. Actual concentrations of holmium and ytterbium ions have been determined using an ICP EM method. Values of  $C_{\text{Ho}} = 0.12$  at.% and  $C_{\text{Yb}} = 0.24$  at.% found are markedly smaller than nominal ones implying small segregation coefficients despite the fact that ionic radii of  $\text{Ho}^{3+}$  and  $\text{Yb}^{3+}$  are inferior to that of  $\text{La}^{3+}$ .

Oriented samples for spectroscopic measurement were cut and polished to record spectra in polarized light.

Optical absorption spectra were acquired with a Varian 5E UV–Vis–NIR spectrophotometer. Spectral bandwidths of the instrument were set to 0.3 nm in the visible region and to 0.5 nm in NIR.

The ambient temperature Raman spectra were measured in the back-scattering arrangement using the Fourier spectrometer—Bruker RFS 100 FT-Raman spectrometer. The 1,064 nm line of Nd:YAG laser was used for an excitation, and signal detection was performed with the D418-T liquid nitrogen-cooled LN–Ge NIR detector. Polycrystalline infrared spectra were measured with a Biorad 575C FT-IR spectrometer in Nujol suspension. Polarized spectra of a single crystal were recorded with a Biorad 575C FT-IR spectrometer by using a fixed-angle specular reflectance accessory. The  $z$  direction is parallel to  $c$  crystallographic axis. The  $y$ -axis is located within the plane perpendicular to the  $c$  period, because this axis is parallel to the twofold axis in the trigonal phase. All spectra have been recorded with a spectral resolution of  $2\text{ cm}^{-1}$ .

To record luminescence spectra, an Argon ion laser, an ozone free DL180-Xe Lamp coupled to an excitation monochromator Dongwoo Optron DM152i and a Apollo Instruments F4-980-6 laser diode emitting infrared radiation at 980 nm were used as excitation sources. Luminescence was dispersed with a Dongwoo Optron DM711 grating monochromator with 750 mm focal length coupled to a Hamamatsu 928 photomultiplier (S-20 spectral response), InGaAs detector and PbS detector, depending on spectral region.

To record luminescence decay curves, an optical parametric oscillator (OPO) pumped with third harmonic of a Nd:YAG laser operating in a pulsed mode was used as an excitation source. Excited luminescence was dispersed by a monochromator and detected with a photomultiplier in the visible and near infrared up to 1,100 nm, whereas a Judson InSb detector was applied to detect infrared emission. Electric signals from detectors were monitored with a Tektronix Model TDS 3052 digital oscilloscope. For spectroscopic measurement at low temperature, the sample was placed in an Oxford Model CF 1204 continuous flow liquid helium cryostat equipped with a temperature controller.

## 3 Results and discussion

Experimental data acquired during this study will be discussed with reference to energy level schemes for  $\text{Ho}^{3+}$  and  $\text{Yb}^{3+}$  ions depicted in Fig. 1. Selected transitions that will be considered in detail are indicated by arrows. Those related to absorption or emission of photons are marked with solid lines. Nonradiative transitions corresponding to

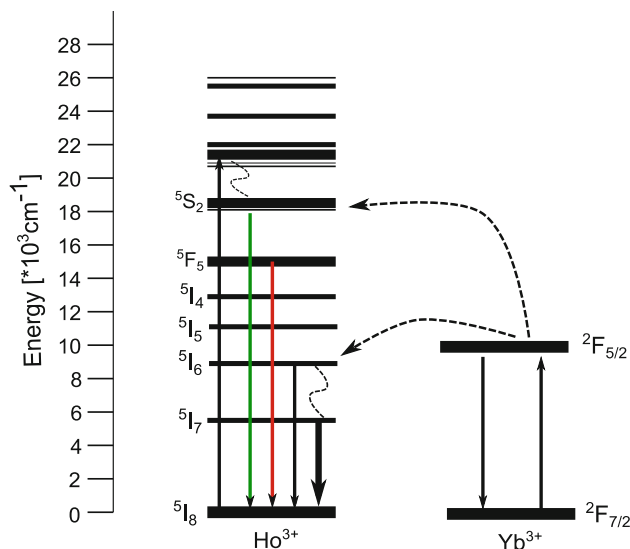
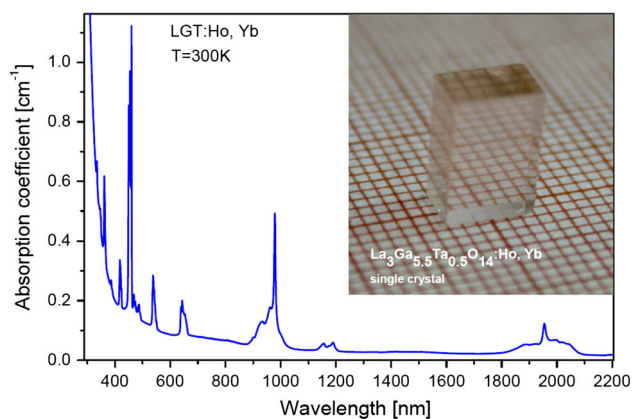


**Fig. 1** Energy level schemes for  $\text{Ho}^{3+}$  and  $\text{Yb}^{3+}$  ions. Selected transitions related to absorption or emission of photons are indicated by *solid arrows*. Nonradiative transitions corresponding to multiphonon relaxation and to nonradiative  $\text{Yb}^{3+}$ - $\text{Ho}^{3+}$  energy transfer are indicated by *dashed arrows*

multiphonon relaxation and to nonradiative  $\text{Yb}^{3+}$ - $\text{Ho}^{3+}$  energy transfer are indicated by dashed lines. Energy levels in Fig. 1 are labelled by symbols  $^{2S+1}L_J$  of corresponding multiplets. Actually, each multiplet is split by the crystal field of LGT into a set of  $2J+1$  crystal field components.

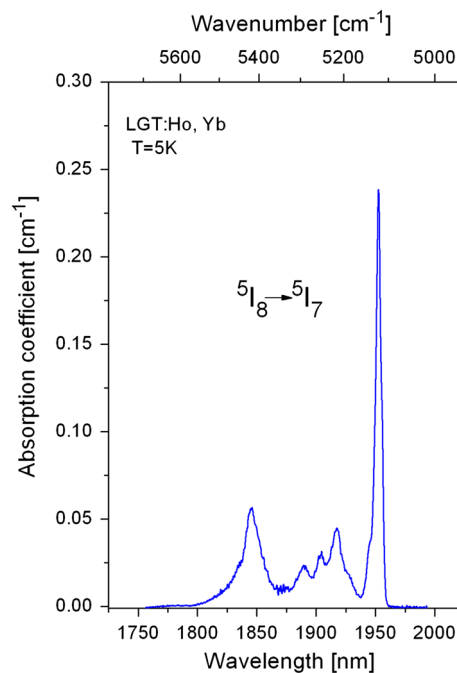
### 3.1 Optical absorption spectra

Figure 2 shows a survey absorption spectrum of LGT:Ho,Yb system recorded at room temperature with unpolarized light propagating along the optical axis of the crystal (axial spectrum). The spectrum is relatively simple since the LGT host absorption obscures  $\text{Ho}^{3+}$  bands at



**Fig. 2** Survey absorption spectrum of LGT:Ho, Yb system recorded at room temperature with unpolarized light propagating along the optical axis of the crystal (axial spectrum) and a photo of  $\text{La}_3\text{Ga}_{5.5}\text{Ta}_{0.5}\text{O}_{14}:\text{Ho}, \text{Yb}$  single crystal sample

wavelengths shorter than 400 nm. In near infrared region, there are two bands relative to the  $\text{Ho}^{3+}$  absorption transitions, namely the  $^5\text{I}_8 \rightarrow ^5\text{I}_7$  transition around 1,950 nm and the  $^5\text{I}_8 \rightarrow ^5\text{I}_6$  transition around 1,170 nm. A more intense band between about 950 nm and 1,100 nm is due to the  $^2\text{F}_{7/2} \rightarrow ^2\text{F}_{5/2}$  transition of  $\text{Yb}^{3+}$ . Expected bands of  $\text{Ho}^{3+}$  transitions to the  $^5\text{I}_5$  and  $^5\text{I}_4$  excited multiplets are missing owing to extremely small transition intensities. Two well-separated bands related to the  $^5\text{I}_8 \rightarrow ^5\text{F}_5$  and to the  $^5\text{I}_8 \rightarrow ^5\text{S}_2$ ,  $^5\text{F}_4$  transitions are centred at 640 and 540 nm, respectively. Finally, between about 520 and 420 nm, the  $\text{Ho}^{3+}$  absorption transitions terminating in the  $^5\text{F}_3$ ,  $^5\text{F}_2$ ,  $^3\text{K}_8$ ,  $^5\text{G}_6$  and  $^5\text{G}_5$  excited multiplets appear. It can be seen that the spectrum shows features characteristic of rare earth ions in crystalline lattices with a certain structural disorder, i.e., large bandwidths and absence of fine structures. The degree of inhomogeneous line broadening cannot be assessed from room temperature absorption spectra since transitions from thermally populated 17 crystal field levels of the ground  $^5\text{I}_8$  multiplet are involved. Recording of spectra at low temperature made it possible to overcome this obstacle. Figure 3 shows the  $^5\text{I}_8 \rightarrow ^5\text{I}_7$  absorption band recorded at 5 K. Supposing that at this temperature solely the lowest crystal field level of the ground multiplet is populated, the energies of crystal field levels of the  $^5\text{I}_7$  excited state can be derived from spectral positions of the band components. Although 15 components are predicted, the spectrum presented in Fig. 3 contains 5 well-defined maxima at 5,419, 5,291, 5,251, 5,215 and 5,124  $\text{cm}^{-1}$ . In addition, two shoulders may be



**Fig. 3** The  $^5\text{I}_8 \rightarrow ^5\text{I}_7$  absorption band of  $\text{Ho}^{3+}$  recorded at 5 K

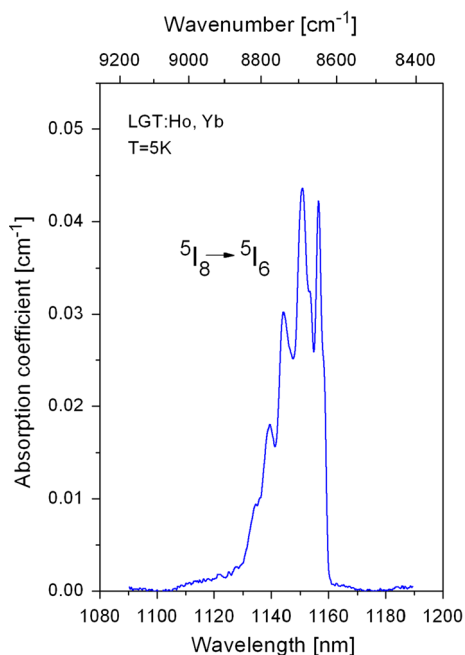


**Fig. 4** The  ${}^5I_8 \rightarrow {}^5I_6$  absorption band of  $\text{Ho}^{3+}$  recorded at 5 K

discerned at 5,188 and 5,142  $\text{cm}^{-1}$ . Figure 4 shows the  ${}^5I_8 \rightarrow {}^5I_6$  band recorded at 5 K. Instead of 13 components predicted, there are solely four maxima at 8,775, 8,740, 8,690 and 8,646  $\text{cm}^{-1}$  and three shoulders at 8,825, 8,668 and 8,633  $\text{cm}^{-1}$ . Table 1 gathers energies of experimental crystal field levels of excited multiplets of  $\text{Ho}^{3+}$  in LGT crystal host derived from 5 K absorption spectra. Low temperature absorption spectra made it possible to assess widths of lines related to transitions between individual crystal field levels. The most narrow line observed has a width (FWHM) of 14  $\text{cm}^{-1}$  a value larger by a factor of ten roughly than those encountered in ordered crystals, for example in  $\text{YVO}_4:\text{Ho}^{3+}$  system [4].

Figure 5 shows the  ${}^2F_{7/2} \rightarrow {}^2F_{5/2}$  absorption band of  $\text{Yb}^{3+}$  recorded at 5 K. Owing to odd number of 4f electrons, the ground  ${}^2F_{7/2}$  multiplet and the  ${}^2F_{5/2}$  excited multiplet of ytterbium are split into four and three crystal field components, respectively. Two narrow lines peaking

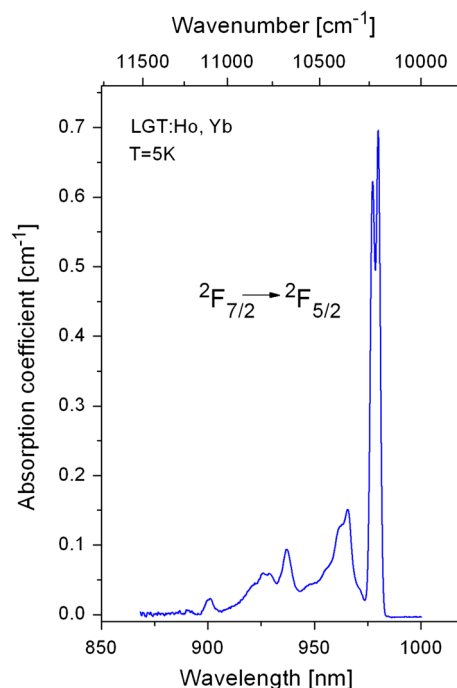


**Fig. 5** The  ${}^2F_{7/2} \rightarrow {}^2F_{5/2}$  absorption band of  $\text{Yb}^{3+}$  recorded at 5 K

at 10,205 and 10,233  $\text{cm}^{-1}$  can be assigned unambiguously to transitions ending on two lowest crystal field components of the excited multiplet, whereas location of third, higher-energy component is rather tentative. It is well known that the electron–phonon coupling is particularly strong in the case of trivalent ytterbium, and therefore, the identification of a no-phonon line in a broad phonon wing stretching from about 10,233 to 11,180  $\text{cm}^{-1}$  is not easy. This problem will be considered later on taking into account the description of LGT lattice vibration in next paragraphs.

$\text{La}_3\text{Ga}_{5.5}\text{Ta}_{0.5}\text{O}_{14}$  crystal host is an optically uniaxial crystal; therefore, optical absorption spectra are expected to show some anisotropy. Indeed, it was found that both the shapes and intensities of all holmium and ytterbium absorption bands depend on incident light polarization. In the following, we will restrict our attention to the  ${}^5I_8 \rightarrow {}^5I_7$  transition of  $\text{Ho}^{3+}$  and  ${}^2F_{7/2} \rightarrow {}^2F_{5/2}$  transition of  $\text{Yb}^{3+}$  that are relevant to a potential infrared laser operation of LGT:Ho, Yb system. Figure 6 compares room temperature absorption bands of the former transition recorded with polarized light having the  $E$  vector perpendicular to the optical axis ( $\sigma$ -spectrum) and with that having the  $E$  vector parallel to the optical axis ( $\pi$ -spectrum). In addition, unpolarized axial spectrum ( $\alpha$ -spectrum) is included in this figure. The spectra stretch from about 1,750 to 2,125 nm and each of them contains a prominent line in the middle. It follows from Fig. 3 that this line is due to transition that bridges the lowest crystal field components of multiplets

**Table 1** Crystal field splitting of low energy excited multiplets of  $\text{Ho}^{3+}$  and  $\text{Yb}^{3+}$  in LGT host derived from 5 K absorption spectra

SLJ	Energy of crystal field levels ( $\text{cm}^{-1}$ )
${}^5I_7$	5,121, 5,142, 5,188, 5,215, 5,251, 5,292, 5,419
${}^5I_6$	8,633, 8,646, 8,668, 8,690, 8,740, 8,775, 8,825
${}^2F_{5/2}$ (Yb)	10,205, 10,233
${}^5F_5$	15,437, 15,540, 15,608, 15,677
${}^5S_2, {}^5F_4$	18,449, 18,471, 18,508, 18,531, 18,566, 18,600, 18,620, 18,689
${}^5F_3$	20,542, 20,612, 20,655, 20,711

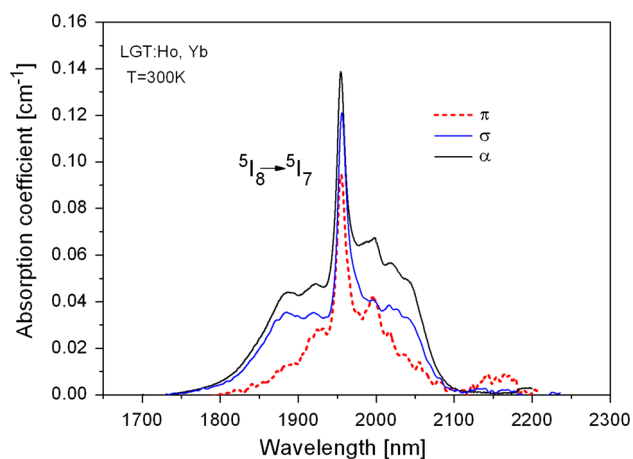


**Fig. 6** Room temperature absorption bands of the  $^5\text{I}_8 \rightarrow ^5\text{I}_7$  transition of  $\text{Ho}^{3+}$  recorded with polarized light having the  $E$  vector perpendicular to the optical axis ( $\sigma$ -spectrum) and parallel to the optical axis ( $\pi$ -spectrum). In addition, unpolarized axial spectrum ( $\alpha$ -spectrum) is included in this figure

involved (0–0 line). Accordingly, the shorter wavelength wing encompasses transitions from the lowest  $^5\text{I}_8$  level to higher-energy components of the  $^5\text{I}_7$ , and the longer wavelength wing is due to transitions from thermally populated crystal field levels of the  $^5\text{I}_8$  multiplet. It can be seen that the two wings are considerably weaker for  $\pi$ -spectrum, whereas axial and  $\sigma$ -spectrum are quite similar. The same measurement procedure was applied to record  $\text{Yb}^{3+}$  absorption spectra presented in Fig. 7. It can be seen in this figure that all spectra shown stretch from 800 to 1,030 nm and are dominated by an intense band component peaking at 980 nm but differ in the spectral distribution of phonon sidebands on the shorter wavelength wings and in overall band intensities. Examination of the

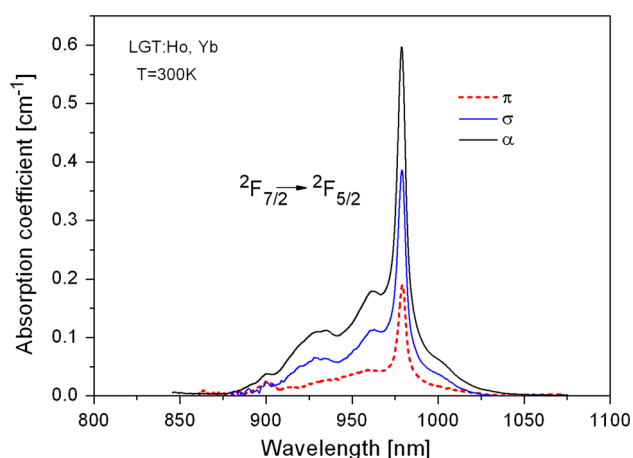


**Fig. 7** Room temperature absorption bands of the  $^2\text{F}_{7/2} \rightarrow ^2\text{F}_{5/2}$  transition of  $\text{Yb}^{3+}$  recorded with polarized light having the  $E$  vector perpendicular to the optical axis ( $\sigma$ -spectrum) and parallel to the optical axis ( $\pi$ -spectrum). In addition, unpolarized axial spectrum ( $\alpha$ -spectrum) is included in this figure

low temperature spectrum in Fig. 5 reveals that the prominent band component at 980 nm in room temperature spectra is due to overlapping 0–0 and 0–1 transitions. Experimental oscillator strengths  $P_{\text{exp}}^k$  were evaluated performing numerical integration of polarized room temperature absorption spectra presented in Figs. 6, 7 and making use of the relation:

$$P_{\text{exp}}^k = \frac{2.303mc^2}{N\pi e^2} \int \alpha_k(\nu) d\nu \quad (1)$$

where  $k$  denotes the status of polarization, i.e.,  $\alpha$ ,  $\pi$  and  $\sigma$ ,  $N$  means the concentration of dopant ions,  $m$ ,  $e$  and  $c$  are the electron mass, electron charge and the velocity of the light, respectively. The symbol  $\alpha$  is the molar absorptivity at the energy  $\nu$  ( $\text{cm}^{-1}$ ).

In this way, values of  $P_{\text{exp}}^\alpha = 3.22 \times 10^{-6}$ ,  $P_{\text{exp}}^\sigma = 2.86 \times 10^{-6}$ ,  $P_{\text{exp}}^\pi = 1.60 \times 10^{-6}$  were obtained for the  $^5\text{I}_8 \rightarrow ^5\text{I}_7$  transition of  $\text{Ho}^{3+}$ , and  $P_{\text{exp}}^\alpha = 4.84 \times 10^{-6}$ ,  $P_{\text{exp}}^\sigma = 4.56 \times 10^{-6}$ ,  $P_{\text{exp}}^\pi = 2.37 \times 10^{-6}$  were obtained for the  $^2\text{F}_{7/2} \rightarrow ^2\text{F}_{5/2}$  transition of  $\text{Yb}^{3+}$  in LGT host. Average  $P_{\text{exp}}^{\text{ave}}$  oscillator strengths defined as  $P_{\text{exp}}^{\text{ave}} = 1/3 P_{\text{exp}}^\alpha + 1/3 P_{\text{exp}}^\sigma + 1/3 P_{\text{exp}}^\pi$  amount to  $2.61 \times 10^{-6}$  and to  $3.92 \times 10^{-6}$  for  $\text{Ho}^{3+}$  and  $\text{Yb}^{3+}$  transitions, respectively. When considering the nature of transitions involved, one should remember that both of them fulfil selection rules for magnetic dipole mechanism, i.e.,  $\Delta L = \Delta S = 0$ ;  $\Delta J = 0, 1$  ( $0 \neq 0$ ). Accordingly, electric dipole and magnetic dipole mechanisms contribute to the transitions. Contribution of magnetic dipole transition  $P_{\text{md}}$  can be assessed based on commonly used relation:

$$P_{\text{md}} = \frac{8\pi m c \nu}{3he^2(2J+1)} n^3 S_{\text{MD}} \quad (2)$$

where  $n$  is the refractive index of the medium,  $J$  denotes the total angular momentum of the initial state,  $c$  means the speed of light in vacuum,  $m$  signifies the mass of an electron,  $e$  represents the electric charge of an electron and  $S_{\text{md}}$  is the transition line strength.

This relation is convenient in that the dependence on the host resides solely in indices of refraction. Taking advantage of oscillator strengths of magnetic dipole transitions for rare earth ions in aqueous solution tabulated in [24] and refraction indices for LGT host tabulated in [14], the values of  $P_{\text{md}} = 4.33 \times 10^{-7}$  and  $P_{\text{md}} = 2.64 \times 10^{-7}$  were calculated for the  $^5\text{I}_8 \rightarrow ^5\text{I}_7$  and  $^2\text{F}_{7/2} \rightarrow ^2\text{F}_{5/2}$  transitions, respectively. Subtraction of  $P_{\text{md}}$  values from  $P_{\text{exp}}$  values provides contributions of electric dipole transitions  $P_{\text{exp}}^{\text{ED}}$ . It follows from these calculations that transitions considered are due essentially to electric dipole mechanism. The contributions of magnetic dipole mechanism to the overall intensities of the  $^5\text{I}_8 \rightarrow ^5\text{I}_7$  transition of  $\text{Ho}^{3+}$  and  $^2\text{F}_{7/2} \rightarrow ^2\text{F}_{5/2}$  transition of  $\text{Yb}^{3+}$  are about 7 and 16 %, respectively.



At this stage of investigation, the suitability of the  $\text{Yb}^{3+}$  absorption band for the purpose of optical pumping with laser diodes may be commented. First, polarized pump light with  $E$  vector perpendicular to the optical axis of the crystal is preferable since high intensity of  $\sigma$ -polarized absorption band would provide better absorption efficiency. Second, prominent band component at 980 nm is advantageously intense, and its spectral position matches perfectly the emission wavelength of commercial InGaAs laser diodes. However, its spectral width is rather small implying that stringent control of a laser diode temperature would be necessary to prevent the pump radiation wavelength from shifting.

### 3.2 Peculiarities of LGT lattice vibrations

Luminescent features of holmium and ytterbium ions in the system under study result from the competition between radiative transitions and nonradiative relaxation processes consisting of multiphonon relaxation and non-radiative energy transfer processes. To account for the contribution of nonradiative processes, the knowledge on spectral characteristics of the host lattice vibrations is of paramount importance. In the following, this issue will be considered in greater detail since peculiarities of LGT lattice vibrations have not been reported before, as far as we know.

The langatate (LGT) crystal crystallizes in the trigonal structure belonging to the  $D_3^2$  (P321) (No. 150) space group as reported in Ref. [8, 19, 20]. The lattice parameters are  $a = 8.228(2)$  and  $c = 5.124(2)$  Å, and the unit cell comprises one formula unit. LGT forms a layer structure of  $\text{GaO}_4$  tetrahedra perpendicular to the crystallographic  $c$ -axis connected through their vertices. These layers in turn are connected by octahedral coordinated  $\text{Ga}^{3+}$  ions and eightfold coordinated  $\text{La}^{3+}$  ions. There are four sites in the crystal structure of LGT in which the Ga(III) atoms share three sites (at  $1a$ ,  $2d$  and  $3f$  Wyckoff position, respectively), La(III) atoms occupy  $3e$  position and Ta(V) substitutes octahedral Ga1 position at  $1a$ . Factor group analysis predicts 66 optical ( $\mathbf{k} = 0$ ) and three acoustic modes of the trigonal  $D_3$  phase distributed among the irreducible representation as follows:  $10A_1 + 12A_2 + 22E$ . The  $A_1$  modes are Raman-active,  $A_2$  modes are IR-active and  $E$  modes are both IR- and Raman-active. Translations of the La and Ga/Ta atoms contribute to  $1A_1 + 2A_2 + 3E$  and  $2A_1 + 4A_2 + 6E$  modes, respectively. Two of these modes  $A_2 + E$  are acoustic, and they are not observed in the IR and Raman spectra. The remaining  $7A_1 + 7A_2 + 14E$  modes correspond to vibrations of oxygen atoms originated from the stretching and bending vibrations as well as the librational modes of the  $\text{GaO}_4$  tetrahedra and  $\text{Ga/TaO}_6$  octahedra.

IR spectra of the LGT crystal are shown in Figs. 8 and 9. Infrared reflectivity for  $E\parallel z$  ( $A_2$  symmetry) and  $E\perp y$  ( $E$  symmetry) polarization is presented in Figs. 8a and 9a, respectively. The IR spectra with a rather big width of the reflection bands show clear LO–TO splitting.

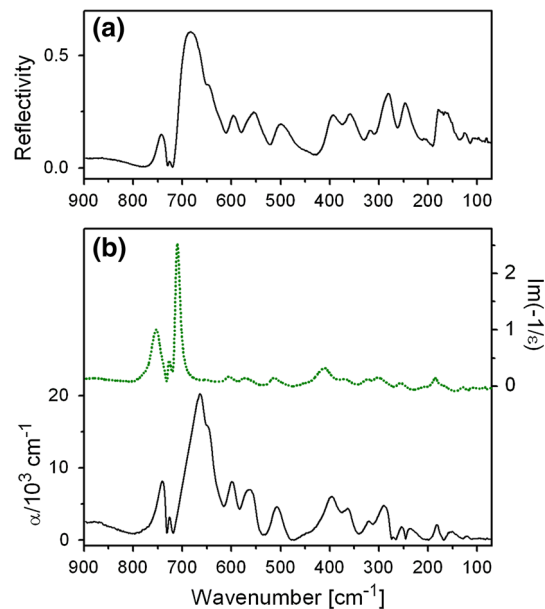


**Fig. 8** **a** Infrared reflectivity data of LGT crystal for  $E\parallel y$  polarization; **b** calculated wavenumber dependence of the absorption coefficient (solid line) and imaginary part of the inverse dielectric function (dotted line)

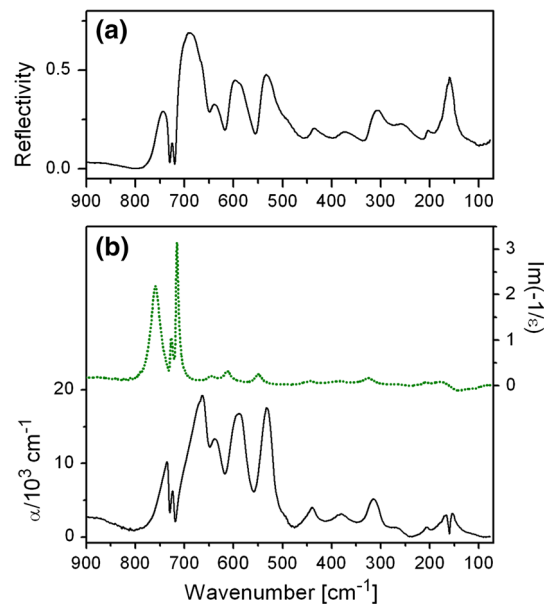


**Fig. 9** **a** Infrared reflectivity data of LGT crystal for  $E\parallel z$  polarization; **b** calculated wavenumber dependence of the absorption coefficient (solid line) and imaginary part of the inverse dielectric function (dotted line)

**Table 2** Observed wavenumbers ( $\text{cm}^{-1}$ ) for IR ( $A_2$  and  $E$ ) and Raman ( $A_1$  and  $E$ ) modes of  $\text{La}_3\text{Ga}_{5.5}\text{Ta}_{0.5}\text{O}_{14}$  together with the proposed assignment (for the IR-active modes, the LO wavenumbers are given in parentheses)

IR		Raman				Assignment	
lly	llz	Polycryst	$x(zz)x - A_1$	$x(yy)x - A_1 + E$	$z(xx)z - A_1 + E$	$x(yz)x - E$	
				790sh			
777sh			778m	778m	778m	776w	Stretching vibrations of tetrahedra
741m (753)	736m (760)	733m	762sh				
726w (727)	724w (727)	693sh	705m	706s	702m	707w	
	670sh			695sh			
664s,b (710)	664s (716)	666vs,b	670vs	670vs	670vs	670m	
645w (652)							
	639m (646)	645s					
599m (605)	590m (612)	594s	600sh			627w	Stretching vibrations of octahedra
564m (575)		570w	590w	590s	590s	589w	
	532m (550)		573w	573sh	572sh	576sh	
				534vw	537vw		
		528s		517sh	509sh		
507m (514)	496sh (497)	493vs	504s	505m	503m	501w	
				492sh	492sh		
454vw				486sh			
446vw	440w (444)		465sh	476w	476m	470m	
	422sh	419sh		464sh	460sh	454sh	
				411vw		386sh	
395m (411)	387w (385)	392m		374sh	381w	375w	Bending vibrations of tetrahedra and octahedra
363m (368)	380w	355m	354m	353s	354s	355w	
320m (324)	315w (326)	314m	320vw	318m	319m	319vs	
				308sh	309sh		
289m (300)		289m	281w	282m	282m		
271sh	269w (270)	282m			277m	274sh	
			261m	262m	260m	261vs	
254w, 236 (256)		252sh	241w	237m	241vs	237s	
		247m					
		214w	211vw	209w		210s	GaO <sub>4</sub> and Ga/TaO <sub>6</sub> units motions and translations
	205w (208)	205w		207sh	199vw	202sh	
			187vw	188sh		188m	
181w (186)	178sh	179w		179w	179s	178sh	
174sh	167, 154w (177)	167w	164sh	168sh			
		158w					
158w (165)		150w	156vw	156vw	158sh	155sh	
150w		140vw	122m	122m	122m	128m	
142w		132w			120sh	123sh	
122vw (128)		126w		114m	112m	113vw	
		122sh	106vw	101m	100s	101vw	
		111w					
102vw	107vw	105sh					
93vw		93vw		91sh	80sh	92sh	
80vw							

Polycryst polycrystalline, vs very strong, s strong, m medium, w weak, vw very weak, b broad, sh shoulder

The Kramers–Kronig analysis was used to transform reflectance spectra into absorbance ones and allows to calculate TO and LO frequencies that are listed in Table 2. The wavenumber dependence of the absorption coefficient and imaginary part of the inverse dielectric function are shown in Figs. 8b and 9b. Polarized Raman spectra of the LGT crystal have been recorded with the back-scattering geometry under the following conditions:  $x(zz)x$  with  $A_1$  symmetry,  $x(yz)x$  with  $E$  symmetry and  $x(yy)x$ ,  $z(xx)z$ ,  $z(yy)z$  and  $z(xy)z$  with both  $A_1$  and  $E$  symmetry. The results are shown in Fig. 10, and the observed wavenumbers are listed in Table 2. The polarized measurements show that the spectra recorded in the  $z(xx)z$ ,  $z(yy)z$  and  $z(xy)z$  polarization configurations are identical (in Fig. 10, the  $z(xx)z$  polarization is only shown). Such depolarization effect is often observed for single crystals with trigonal symmetry.

The mode symmetry assignment can be achieved by comparison with the results for other compounds where tetrahedral and octahedral oxygen polyhedra are formed [21–23]. The bands observed in the region between 630 and 800  $\text{cm}^{-1}$  are stretching modes of tetrahedra, whereas bands observed at 450–600  $\text{cm}^{-1}$  are stretching modes of octahedra. The modes observed in the range of 230–430  $\text{cm}^{-1}$  are bending modes, some of them involve large contribution from motions of nearly rigid  $\text{GaO}_4$  or  $\text{GaO}_6$  units. Translational and librational modes contribute significantly to the modes below 230  $\text{cm}^{-1}$ . Because the crystal structure is built of different kind of oxygen polyhedra not independent of each other and the lower frequency range is densely populated with modes of different symmetries, it is difficult to assign all modes exactly, and they may overlap themselves and additionally the bending mode region.

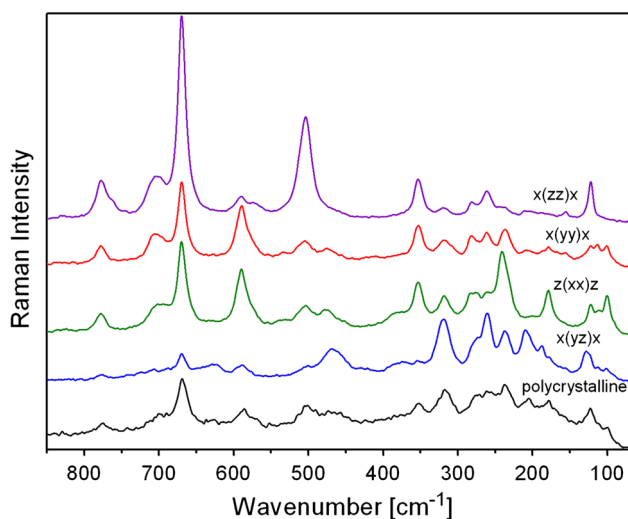


**Fig. 10** Raman spectra of LGT polycrystalline and single crystal for  $x(zz)x$ ,  $x(yy)x$ ,  $z(xx)z$  and  $x(yz)x$  polarizations

Some of Raman bands are rather broad, and the number of observed Raman and IR bands for a respective polarization is bigger than that predicted by the factor group analysis. The bands are not fully polarized maybe due to defects or a slight mismatch in the orientation of the sample in respect to the electric vector of the polarized laser light. A certain relaxation of the selection rules may be due to a structural disorder that occurs in this crystals since pentavalent  $\text{Ta}^{5+}$  ions occupy octahedral Ga(1) sites together with trivalent  $\text{Ga}^{3+}$  ions. It follows from Table 2 that the LGT host shows a rich phonon spectrum with the cut-off phonon energy close to 778  $\text{cm}^{-1}$ .

### 3.3 Luminescence spectra

Luminescence related to transitions originating in the  $^5S_2$ ,  $^5F_5$ ,  $^5I_6$  and  $^5I_7$  excited multiplets of  $\text{Ho}^{3+}$  and in the  $^2F_{5/2}$  excited multiplet of  $\text{Yb}^{3+}$  in LGT host crystal was observed. Figure 11 shows a survey unpolarized luminescence spectrum recorded at room temperature in the 500–1,300 nm spectral region. Excitation was provided by an Argon ion laser emitting at 457.9 nm. Luminescence bands peaking at 540, 750 and 1,025 nm are assigned to the  $^5S_2 \rightarrow ^5I_8$ ,  $^5S_2 \rightarrow ^5I_7$  and  $^5S_2 \rightarrow ^5I_6$  transitions, respectively. Relatively weaker band around 650 nm is assigned to the  $^5F_5 \rightarrow ^5I_8$  transition, and a quite intense band near 1,180 nm is assigned to the  $^5I_6 \rightarrow ^5I_8$  transition. A very weak feature that appears around 980 nm, on the short wavelength side of the  $^5S_2 \rightarrow ^5I_6$  band, has been assigned to the  $^2F_{5/2} \rightarrow ^2F_{7/2}$  transition of  $\text{Yb}^{3+}$  based on the comparison of luminescence decays after a short pulse excitation. To corroborate this finding, the  $^2F_{5/2} \rightarrow ^2F_{7/2}$  luminescence spectrum was recorded when exciting the  $^5F_5$  level of  $\text{Ho}^{3+}$  with a 660 nm light emitted by a red diode laser. Inset in Fig. 11 shows details of the spectrum acquired. The  $\text{Yb}^{3+}$  luminescence is weak, but it contributes to the spectrum implying that the nonradiative energy transfer from holmium ions to ytterbium ions takes place. Fortunately, energy transfer in the reverse direction appears to be quite efficient. Indeed, the  $^5I_7 \rightarrow ^5I_8$  emission was observed when pumping with a laser diode emitting radiation at 980 nm. This observation is encouraging in view of small concentrations of interacting ions. Figure 12 compares room temperature polarized  $^5I_7 \rightarrow ^5I_8$  emission spectra excited at 980 nm. They differ in the overall intensity, but their shapes are similar. Anisotropy of this luminescence band is reminiscent of that revealed in the absorption spectrum. It can be seen in Fig. 12 that band intensities are expressed quantitatively in units of emission cross section. A two-step calculation procedure was applied for this purpose. First, the rate of the  $^5I_7 \rightarrow ^5I_8$  radiative transition  $A_{ED}$  was evaluated making use of relation:



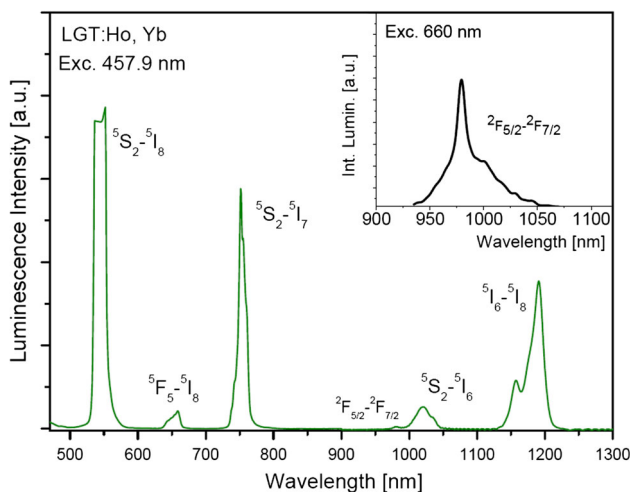


**Fig. 11** Survey room temperature unpolarized luminescence spectrum excited at 457.9 nm and recorded in the 500–1,300 nm spectral region. *Inset* shows details of the Yb<sup>3+</sup> luminescence spectrum recorded upon excitation into the <sup>5</sup>I<sub>8</sub> → <sup>5</sup>F<sub>5</sub> absorption band of Ho<sup>3+</sup> around 660 nm

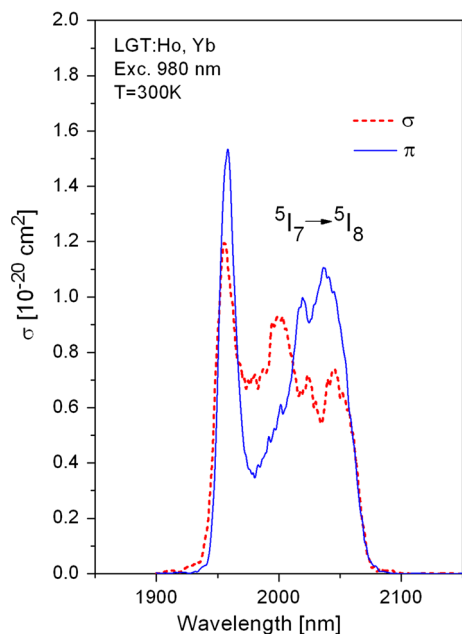


**Fig. 12** Room temperature polarized <sup>5</sup>I<sub>7</sub> → <sup>5</sup>I<sub>8</sub> emission spectra acquired upon excitation at 980 nm

$$A_{ED} = \frac{8\pi^2 e^2 n^2}{mc\lambda^2} \times \frac{2J' + 1}{2J + 1} \times P_{exp}^{ED} \tag{3}$$

where *n* is the refractive index, the values of *J'* and *J* are 7 and 8, respectively,  $\lambda$  denotes emission wavelength and  $P_{exp}^{ED}$  is the value of the electric dipole oscillator strength. Symbols *e*, *m* and *c* denote electron charge, electron mass and speed of light, respectively. In this way, the  $A_{ED} = 167 \text{ s}^{-1}$  was determined. Contribution of the

magnetic dipole transition rate was calculated in accordance with the following formula:

$$A_{MD} = \frac{64\pi^4 v^3}{3h(2J + 1)} n^3 S_{MD} \tag{4}$$

where  $S_{MD}$  is the magnetic dipole line strength. In relation to that  $A_{MD} = 19 \text{ s}^{-1}$  and total radiative transition rate  $A_{tot} = A_{ED} + A_{MD}$  equals to  $186 \text{ s}^{-1}$ .

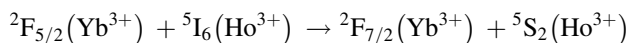
Next, the experimental emission spectra were calibrated in units of the cross section  $\sigma_k^{em}(\lambda)$ , applying the Füchtbauer–Ladenburg formula:

$$\sigma_k^{em}(\lambda) = \frac{3\beta\lambda^4 I_k(\lambda)}{8\pi n_k^2 c \tau_{rad} \int [I_\sigma(\lambda) + I_\pi(\lambda)] d\lambda} \tag{5}$$

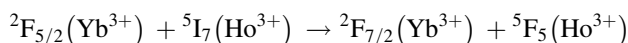
where  $I(\lambda)$  represents the experimental emission intensity at the wavelength  $\lambda$ , *c* is the light velocity, *n*,  $\beta$  and  $\tau_{rad}$  denote the refractive index, branching ratio and radiative lifetime, respectively. The sign *k* relates to the  $\sigma$  and  $\pi$  parameters. In the case of uniaxial crystal,  $n_k$  means either  $n_\sigma = n_o$  or  $n_\pi = n_e$ .

It can be seen in Fig. 12 that in the spectral region above 2,000 nm, there is a local maximum in  $\pi$ -polarized spectrum. Its peak value of  $1.1 \times 10^{-20} \text{ cm}^2$  located at 2,038 nm is smaller than those reported for other holmium-doped crystals. For a comparison, reported peak emission cross section values (in units  $10^{-20} \text{ cm}^2$ ) for  $\pi$ -polarized <sup>5</sup>I<sub>7</sub> → <sup>5</sup>I<sub>8</sub> spectra amount to 1.45 (at 2,047 nm) for NaBi(WO<sub>4</sub>)<sub>2</sub>:Ho [25], 1.55 (at 2,051) for YLi<sub>4</sub>:Ho [26], 1.67 (at 2,045 nm) for LiGd(MoO<sub>4</sub>):Tm,Ho [27] and 2.5 (at 2,030) for YVO<sub>4</sub>:Ho [4] systems.

When recording Ho<sup>3+</sup> emission excited at 980 nm, a weak up-converted green luminescence was observed. A log–log plot of its integrated intensity versus power of incident infrared radiation is presented in Fig. 13. In the inset, there is a spectrum of up-converted emission containing a green <sup>5</sup>S<sub>2</sub> → <sup>5</sup>I<sub>8</sub> band and considerably weaker <sup>5</sup>F<sub>5</sub> → <sup>5</sup>I<sub>8</sub> band. The plot in Fig. 13 is consistent with a straight line with a slope of 1.73 indicating that a two-step energy transfer process is involved in the up-conversion phenomenon. Its mechanism, well documented in numerous crystals and glasses co-doped with holmium and ytterbium, consists of two consecutive acts of Yb<sup>3+</sup>–Ho<sup>3+</sup> energy transfer. In the first step, an excitation energy of the <sup>2</sup>F<sub>5/2</sub> level of Yb<sup>3+</sup> is transferred nonradiatively to the <sup>5</sup>I<sub>6</sub> level of Ho<sup>3+</sup>. In the second step, the <sup>5</sup>S<sub>2</sub> level is populated via the <sup>5</sup>I<sub>6</sub> intermediate level according to the scheme:



The <sup>5</sup>F<sub>5</sub> may be populated via the <sup>5</sup>I<sub>7</sub> intermediate level according to the scheme:



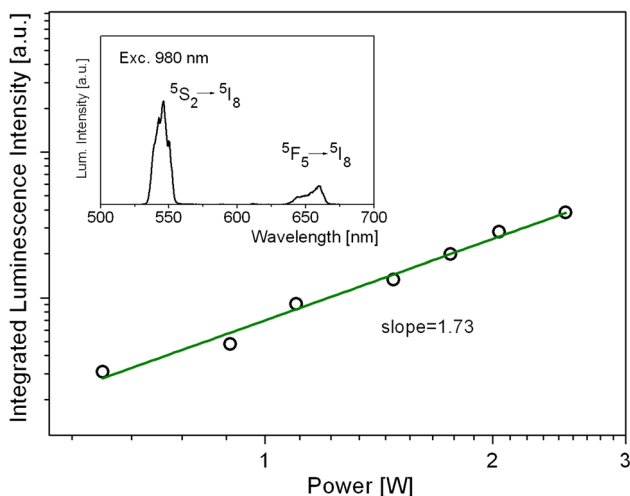


**Fig. 13** A log–log plot of integrated intensity of up-converted green emission versus power of incident infrared radiation at 980 nm. *Inset* shows a spectrum of up-converted emission recorded in the 500–700 nm spectral region

provided that the rate of intra-ion  ${}^5I_6 \rightarrow {}^5I_7$  transition is sufficient to feed the  ${}^5I_7$  level of  $\text{Ho}^{3+}$ .

The colour of up-converted emission in  $\text{Yb}^{3+} + \text{Ho}^{3+}$  co-doped hosts depends on the competition between these two schemes. A governing factor is the  ${}^5I_6$  lifetime. When the  ${}^5I_6$  level is short-lived due to a high multiphonon relaxation rate, a red up-converted emission related to the  ${}^5F_5 \rightarrow {}^5I_8$  is observed, as is the case of  $\text{YVO}_4:\text{Ho}, \text{Yb}$  [4]. Otherwise, a green emission occurs. Our results indicate that the lifetime of the  ${}^5I_6$  level of  $\text{Ho}^{3+}$  in LGT host is quite high. It should be noticed here that pairs of transition in the second steps written above fulfil requirements of energy conservation. Examination of energy level scheme in Fig. 1 and of experimental data in Table 1 leads to the conclusion that first step do not fulfil conditions of resonance and proceeds with an assistance of phonons.

Unlike the phenomena of up-conversion discussed above, the mechanisms involved in a down-converted  $\text{Yb}^{3+}$  emission are not obvious. A process involving a cascade multiphonon relaxation via the  ${}^5S_2$ ,  ${}^5F_5$  and  ${}^5I_4$  levels is able to feed the  ${}^5I_5$  level. Subsequent phonon-assisted energy transfer from the  ${}^5I_5$  level of  $\text{Ho}^{3+}$  to the  ${}^2F_{5/2}$  level of  $\text{Yb}^{3+}$  is likely to occur. Reversed second steps responsible for up-conversion phenomena may be relevant, too.

### 3.4 Excited state relaxation dynamics

To characterize the relaxation dynamics of excited states involved in luminescence phenomena discussed above, we recorded decay curves of luminescence originating in the  ${}^5S_2$ ,  ${}^5F_5$ ,  ${}^5I_6$ ,  ${}^5I_7$  levels of  $\text{Ho}^{3+}$  and the  ${}^2F_{5/2}$  level of  $\text{Yb}^{3+}$ .

**Table 3** Experimental room temperature lifetimes for luminescent levels of  $\text{Ho}^{3+}$  and  $\text{Yb}^{3+}$  in LGT host

SLJ	Lifetime ( $\mu\text{s}$ )
${}^5S_2$	75
${}^5F_5$	3
${}^5I_6$	450
${}^5I_7$	4,970
${}^2F_{5/2}$ (Yb)	643

In this measurement, the levels in question were excited directly employing short light pulses delivered by appropriately tuned OPO. It was found that all recorded luminescence decay curves are consistent with a single exponential time dependence. Table 3 gathers values of luminescence lifetime determined from decay curves recorded at room temperature. Experimental luminescence lifetime  $\tau_{\text{exp}}$  of an excited level, derived from a luminescence decay curve, is an inverse of a rate  $A_{\text{tot}}$  encompassing a sum of rates related to all decay contributions. In particular,  $A_{\text{tot}}$  value for an excited state of rare earth ions in crystals is a sum of radiative transition rates  $A_r$ , multiphonon relaxation rate  $A_{\text{mph}}$  and of decay rate  $A_{\text{ET}}$  due to nonradiative energy transfer between interacting ions. In principle, evaluation of contributing decay rates is not straightforward. In the following, we will restrict our attention to the relaxation of the  ${}^5I_7$  level of  $\text{Ho}^{3+}$  and the  ${}^2F_{5/2}$  level of  $\text{Yb}^{3+}$  because of their relevance to a potential laser-diode-pumped laser operation near 2  $\mu\text{m}$ . The rate  $A_r = 186 \text{ s}^{-1}$  of the  ${}^5I_7 \rightarrow {}^5I_8$  radiative transition was calculated above using the relations (3, 4). The  ${}^5I_7$  radiative lifetime defined as an inverse of radiative transition rate amounts thus to 5.4 ms, whereas a value of 4.97 ms was determined experimentally from luminescence decay curve. Taking into account that both these values suffer from an experimental incertitude, the agreement between measured and calculated values is reasonable and implies small contribution of nonradiative relaxation to the  ${}^5I_7$  decay. In fact, it follows from the “energy gap law” that the rate of multiphonon relaxation involving simultaneous emission of six phonons with the cut-off energy of  $778 \text{ cm}^{-1}$  that are needed to bridge an energy difference between the  ${}^5I_7$  and  ${}^5I_8$  multiplets is predicted to be low.

Inserting the oscillator strength values determined in previous subsection, the  $A_{\text{ED}} = 1,422 \text{ s}^{-1}$  and  $A_{\text{MD}} = 98 \text{ s}^{-1}$  were obtained for the  ${}^2F_{5/2} \rightarrow {}^2F_{7/2}$  transition of  $\text{Yb}^{3+}$ . It follows from these calculations that the total radiative transition rate  $A_r = 1,520 \text{ s}^{-1}$  and the  ${}^2F_{5/2}$  radiative lifetime amounts to 660  $\mu\text{s}$ . Relaxation of the  ${}^2F_{5/2}$  level of  $\text{Yb}^{3+}$  is governed by radiative transitions and experimentally evidenced nonradiative  $\text{Yb}^{3+}-\text{Ho}^{3+}$  energy transfer. Close agreement between values of calculated radiative lifetime and measured lifetime indicates that the calculated value is likely to be underestimated. It should be

noticed here that concentrations of  $\text{Yb}^{3+}$  and  $\text{Ho}^{3+}$  ions are very small, and hence, the contribution of  $\text{Yb}^{3+}$ – $\text{Ho}^{3+}$  energy transfer rate to the overall relaxation rate of  $\text{Yb}^{3+}$  is not large enough to be determined in view of uncertainty of experimental data.

#### 4 Summary and conclusions

Measurement of spectroscopic features of LGT:Ho, Yb single crystal, encompassing IR host absorption spectra and Raman spectra at room temperature, optical absorption and luminescence spectra of  $\text{Ho}^{3+}$  and  $\text{Yb}^{3+}$  at room temperature and at 5 K, and luminescence decay curves at room temperature was done. Results gathered provide a fundamental information about energy distribution of the host lattice vibrations, characteristics of spectral bands, transitions intensities and excited state relaxation dynamics of the system under study. In particular, bands of IR host absorption as well as of absorption and emission of incorporated luminescent ions show important inhomogeneous spectral broadening as a consequence of a certain structural disorder inherent to the crystal lattice in which pentavalent  $\text{Ta}^{5+}$  ions occupy octahedral Ga(1) sites together with trivalent  $\text{Ga}^{3+}$  ions. The cut-off phonon energy of about  $780\text{ cm}^{-1}$  is low enough to assure high quantum efficiency of the  ${}^2\text{F}_{5/2}$  level of  $\text{Yb}^{3+}$  and the  ${}^5\text{I}_7$  level of  $\text{Ho}^{3+}$  ions. Based on the obtained results, principal merits and shortcoming of the system under study with regard to its potential laser operation near  $2\text{ }\mu\text{m}$  may be pointed out. In particular, the relatively long  ${}^5\text{I}_7$  lifetime of about 5 ms combined with a moderate value of emission cross section for the  ${}^5\text{I}_7 \rightarrow {}^5\text{I}_8$  transition indicates that we are dealing with an intermediate-gain laser material. Despite important inhomogeneous spectral broadening, the  ${}^5\text{I}_7 \rightarrow {}^5\text{I}_8$  emission band is narrow with an overall bandwidth of 175 nm since crystal field splitting of multiplets involved is rather small. Nevertheless, smooth emission band is favourable in that the potential laser wavelength can be tuned within width of emission band. Observed marked anisotropy of the  ${}^5\text{I}_7 \rightarrow {}^5\text{I}_8$  emission band implies that polarized output laser radiation can be easily obtained. In view of low concentrations of interacting  $\text{Yb}^{3+}$  and  $\text{Ho}^{3+}$  ions, the rate of energy transfer from ytterbium to holmium could not be assessed quantitatively. Nevertheless, observed feasibility of feeding the  ${}^5\text{I}_7$  level of  $\text{Ho}^{3+}$  upon excitation of  $\text{Yb}^{3+}$  ions is encouraging. On the other hand, an adverse up-conversion process was observed at these low doping levels, too. To assess the competition between the energy transfer processes that occur in this system, an examination of excited state excitation and relaxation dynamics in LGT crystals

containing higher doping levels is needed. In our opinion, the main shortcoming of the material under study is related to very low segregation coefficient for the incorporation of ytterbium and holmium ions. Czochralski growth of LGT crystals with uniform distribution of  $\text{Yb}^{3+}$  and  $\text{Ho}^{3+}$  and higher concentrations may pose serious problems.

#### References

1. A. Diening, S. Kueck, *J. Appl. Phys.* **87**, 4063 (2000)
2. J. Li, J. Wang, H. Tan, X. Chen, F. Song, H. Zhang, S. Zhao, *J. Cryst. Growth* **256**, 324 (2003)
3. V. Jambunathan, X. Mateos, M.C. Pujol, J.J. Carvajal, M. Aguilo, F. Diaz, *Phys. Procedia* **8**, 162 (2010)
4. R. Lisiecki, G. Dominiak-Dzik, W. Ryba-Romanowski, T. Łukasiewicz, *J. Appl. Phys.* **96**, 6323 (2004)
5. H. Dong–Dong, Y. Qiu–Hong, W. Yong–Gang, Z. Hao–Jia, L. Shen–Zhou, ZYu–Wan Shen–Zhou, L. Yu–Wan, W. Zhi–Yi, *Chin. Phys. B* **22**, 037801 (2013)
6. S. Balaji, A.D. Sontakke, R. Sen, A. Kalyandurg, *Opt. Mater. Express* **1**, 138 (2011)
7. R. Xu, J. Pan, L. Hu, J. Zhang, *J. Appl. Phys.* **108**, 043522 (2010)
8. H. Takeda, K. Sugiyama, K. Inava, K. Shomamura, T. Fukuda, *Jpn. J. Appl. Phys.* **36**, L919 (1997)
9. H. Fuks, S.M. Kaczmarek, M. Berkowski, *Phys. Stat. Solidi (a)* **203**, 3640 (2006)
10. G.M. Kuzmicheva, J.A. Kaurova, V.B. Rybakov, S.S. Khasanov, A. Cousson, O. Zaharko, E.N. Domoroschina, A.B. Dubovsky, *Cryst. Res. Techn.* **47**, 131 (2012)
11. I.A. Kaurova, G.M. Kuzmicheva, A.B. Dubovsky, *Inorg. Mater.* **46**, 1131 (2010)
12. J. Bohm, E. Chilla, C. Flannery, H.-J. Froehlich, T. Hauke, R.B. Heimann, M. Hengst, U. Straube, *J. Cryst. Growth* **216**, 293 (2000)
13. J. Luo, D. Shah, C.F. Klemenz, M. Dudley, H. Chen, *J. Cryst. Growth* **287**, 300 (2006)
14. J. Stade, L. Bohaty, M. Hengst, R.B. Heimann, *Cryst. Res. Techn.* **37**, 1113 (2002)
15. A.A. Kaminskii, G.R. Verdun, B.V. Mill, A.V. Butashin, *Neorg. Mater.* **27**, 141 (1992)
16. W. Ryba-Romanowski, G. Dominiak-Dzik, P. Solarz, *Mol. Phys.* **101**, 1067 (2003)
17. S. Georgescu, A.M. Voiculescu, O. Toma, L. Gheorghe, C. Matei, S. Hau, *Optoelectron. Adv. Mater. Rapid Commun.* **4**, 1937 (2010)
18. S. Georgescu, A.M. Voiculescu, C. Matei, R. Birjega, I. Petrescu, *Phys. B* **407**, 1124 (2012)
19. J. Bohm, R.B. Heimann, M. Hengst, R. Roewer, J. Schindler, *J. Cryst. Growth* **204**, 128 (1999)
20. G.M. Kuzmicheva, E.A. Tyunina, E.N. Domoroschina, V.B. Rybakov, A.B. Dubovskii, *Inorg. Mater.* **41**, 412 (2005)
21. G.D. Saraiva, W. Paraguassu, M. Mączka, P.T.C. Freire, F.F. de Sousa, J. Mendes Filho, *J. Raman Spectrosc.* **42**, 1114 (2011)
22. L. Macalik, J. Hanuza, A.A. Kaminskii, *J. Molecular Struct.* **555**, 289 (2000)
23. M. Mączka, M. Ptak, A. Majchrowski, J. Hanuza, *J. Raman Spectrosc.* **42**, 209 (2011)
24. C. Görller-Walrand, K. Binnemans (1998). Chapter 167 spectral intensities of f–f transitions, in *Handbook on the Physics and*

- Chemistry of Rare Earths* Elsevier Science BV, Po box 211, 1000 AE Amsterdam, Netherlands, 101–264
25. A. Méndez-Blas, M. Rico, V. Volkov, C. Zaldo, C. Cascales, *Phys. Rev. B* **75**, 174208 (2007)
  26. J. Tang, Y. Chen, Y. Lin, X. Gong, J. Huang, Z. Luo, Y. Huang, *Opt. Mater. Express* **2**, 1064 (2012)
  27. B.M. Walsh, N.P. Barnes, M. Petros, J. Yu, U.N. Singh, *J. Appl. Phys.* **95**, 3255 (2004)